A Geochemical approach to evolution of granitic plutons: a case study, the acid intrusions of Punta Falcone (Northern Sardinia, Italy)

Chemical Geology, 92 (1991) 87–105
Elsevier Science Publishers B.V., Amsterdam

A geochemical approach to the evolution of granitic plutons: a case study, the acid intrusions of Punta Falcone (northern Sardinia, Italy)

G. Poli and S. Tommasini
Department of Earth Sciences, Piazza Università, 06100 Perugia, Italy

(Received February 15, 1990; revised and accepted September 15, 1990)

ABSTRACT

Poli, G. and Tommasini, S., 1991. A geochemical approach to the evolution of granitic plutons: a case study, the acid intrusions of Punta Falcone (northern Sardinia, Italy). In: A. Peccerillo (Guest-Editor), Geochemistry of Granitoid Rocks. Chem. Geol., 92: 87–105.

A group of small granitic stocks outcrop in an area of 4 km^2 at Punta Falcone (northern Sardinia, Italy). The stocks, which belong to the Sardinia Corsica Batholith, were emplaced during the late tectonic phase of the Hercynian orogeny. Detailed field observations, and studies of the petrography, mineral- and whole-rock geochemistry were carried out on these stocks: systematic differences in both whole-rock and mineral compositions were found between the stocks.

The granitic stocks which outcrop in the southwestern and northern sector of the Punta Falcone area were examined but briefly since they have fairly homogeneous compositions. The granitic stock which outcrops in the central sector, on the other hand, shows evidence of a complex evolutionary history. This intrusion shows compositional zoning from granodiorite to leucogranite. A two-stage model for the evolution of granitic magmas by an unmixing process between a solid and a liquid phase within a single magmatic batch is proposed on the basis of the geochemical characteristics of this granitic stock. In the first stage, the parental magma undergoes a 30–35% in-situ fractional crystallization, developing the solid and liquid phases represented by early crystallized minerals and residual liquid, respectively. Then, in the second stage, the relative proportions of the solid and liquid phases are modified by a filter pressing segregation mechanism which squeezes the liquid phase inward to the centre of the intrusion. Therefore, each sample represents a mixture between the early crystallized mineralogic assemblage (solid phase) and the residual liquid (liquid phase).

The bulk chemical composition of the liquid phase was determined using bivariate diagrams with Sr as differentiation index. The bulk chemical composition of the solid phase was computed using a self-consistent "feedback system" which handles variations in the modal composition of the solid phase accompanied by variations in trace-element bulk distribution coefficients.

1. Introduction

Several processes have been proposed to explain the geochemical variations observed in granitoid plutons. White and Chappell (1977) suggested the *restite unmixing* model as the main process responsible for such variations; however, recently, Wall et al. (1987) critically examined the restite model and found that criteria for the recognition of restite components are equivocal. McCarthy et al. (1976, 1978a, b) proposed a fractional crystallization process for the evolution of granitic magmas on the basis of Ba, Rb, Sr distributions in granites. An *in-situ fractional crystallization* process has been suggested by Tindle and Pearce (1981) and Michael (1984) to explain the origin of extremely evolved felsic magmas. Furthermore, a model combining the effects of convective circulation and Soret diffusion (*thermogravitational diffusion* model) has been suggested to explain the origin of chemi-

cally zoned magma chambers (Shaw et al., 1976; Hildreth, 1979, 1981).

In this paper, following the model proposed by Sultan et al. (1986), a geochemical approach is suggested to understand the evolution of granitic plutons which display a particular evolutionary path. The model has been developed studying a small, zoned, granitoid intrusion (ca. 2.5 km^2) outcropping in the Punta Falcone area (northern Sardinia, Italy). The petrographical, geochemical, and mineral chemistry study of the differentiation history of this stock is consistent with a model for the evolution of granitic magmas by an *unmixing* process between a solid and a liquid phase within a single magmatic batch. The other stocks outcropping in the Punta Falcone area were examined but briefly, owing to their quite homogeneous compositions.

2. Geological setting

The Sardinia–Corsica Batholith, located in the Mediterranean Sea, west of Italy, was emplaced during the tectono-metamorphic evolution of the Hercynian orogeny. Several granitoid intrusions were emplaced during both syn-tectonic and post-tectonic phases, covering a span of time from 320 Ma to about 280 Ma. These plutons intruded the metamorphic sequences of Sardinia–Corsica basement. In Sardinia, the intrusive sequence ranges in composition from gabbroic to leucogranitic plutons, with a large predominance of monzogranitic and granodioritic plutons (see Ghezzo and Orsini, 1982; Poli et al., 1989, for a review). The plutons of the Punta Falcone area are a typical calc-alkaline, I-type suite (Ghezzo and Orsini, 1982). In this area, of approximately 4 km^2, four granitic intrusions have been recognized, with sharp contacts between them (Tommasini, 1987). These stocks intrude metamorphic rocks of amphibolite facies (Bralia et al., 1982) which outcrop in the southeastern sector of the area (Fig. 1).

The Gr-I stock outcrops in the central sector of the Punta Falcone area (Fig. 1). On petrographical and geochemical grounds, three main facies have been distinguished in the Gr-I stock (Fig. 1): facies A, B, and C, composed of granodiorites, monzogranites, and leucocratic syeno-monzogranites, respectively. These facies display a roughly concentric zoning and exhibit transitional contacts. A zone rich in aplite pegmatite is also developed along the northern edge of the Gr-I outcrop area.

In contrast, the granitic stocks which outcrop in the southwestern (Gr-II), and in the northern (Gr-III) sectors of the Punta Falcone area (Fig. 1), are quite homogeneous and do not exhibit any significant zoning. The granitic stock (Gr-IV) which outcrops in the northeast of the Punta Falcone area (Fig. 1), is characterized by the presence of magmatic flow lineations defined by K-feldspar megacrysts, and by numerous rounded mafic enclaves. It is noteworthy that mafic enclaves are absent in the other stocks, suggesting that Gr-IV underwent a different evolutionary history. Structural analyses of the contacts among the stocks indicate that the sequence of emplacement began with the Gr-I intrusion, followed by the intrusion of the Gr-II and Gr-III. The absence of contacts between the latter stocks (Fig. 1) does not allow the relative timing of their emplacement to be established. The Gr-IV stock marked the end of the intrusive sequence.

In the Punta Falcone area, a stratified gabbroic complex also outcrops (Fig. 1), its emplacement being coeval with that of the Gr-I stock. The physico-chemical processes of interaction between the gabbroic complex and the Gr-I stock have been extensively studied (see Bralia et al., 1982; Poli et al., 1989; Poli and Tommasini, 1989, for a review). A dyke swarm, trending 20°–30° N, crosscuts all the Punta Falcone intrusions. The dyke swarm consists of both diabases and granitic porphyries and may be linked to the last period of magmatic activity of Hercynian orogenesis on the islands of Sardinia and Corsica.

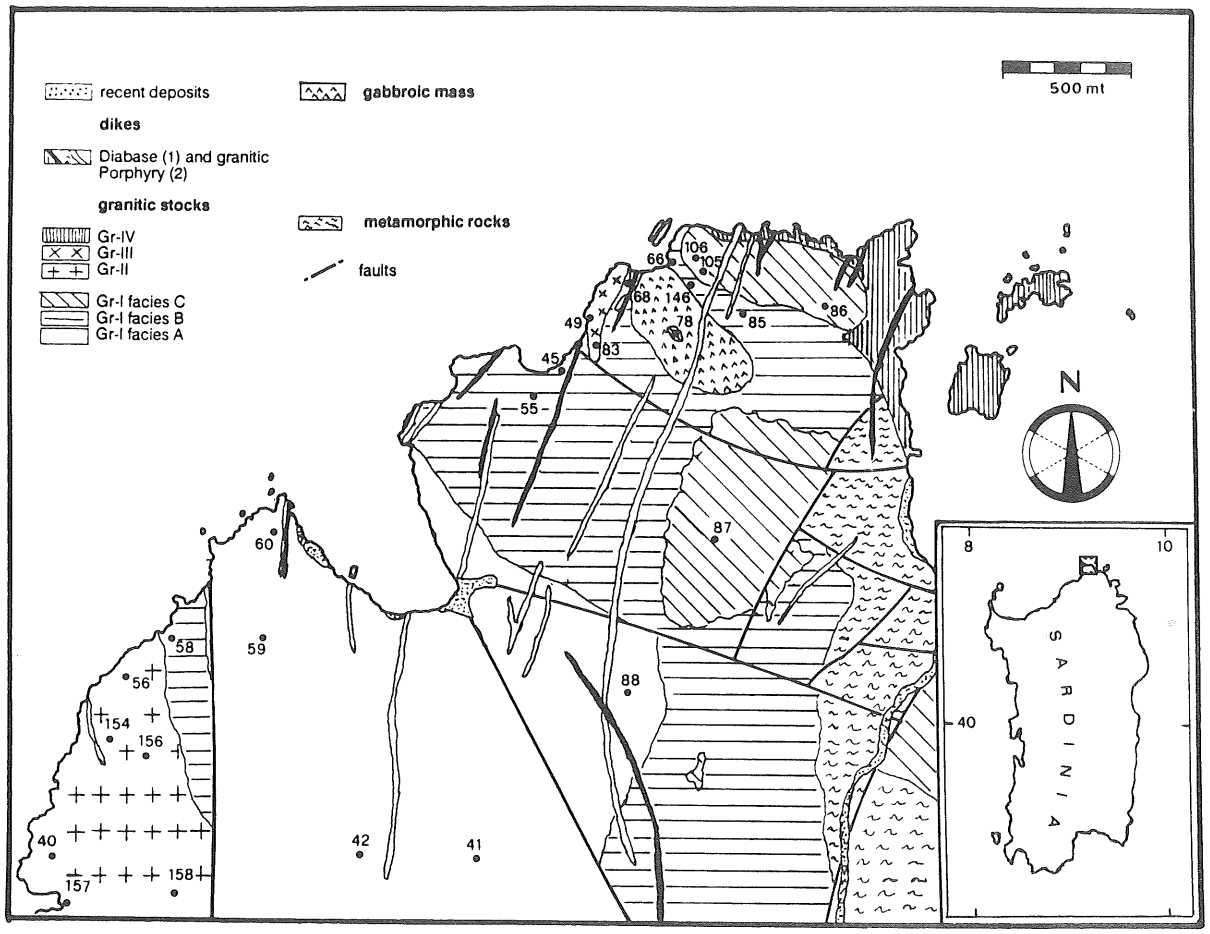

Fig. 1. Geological sketch map of the Punta Falcone area (after Tommasini, 1987), and location of samples.

3. Petrography and mineral chemistry

According to the normative classification of Streckeisen and Le Maitre (1979), the Gr-I samples range from granodiorites (facies A) to monzogranites (facies B), and leucocratic syeno-monzogranites (facies C) (Fig. 2). Gr-II samples are mainly monzogranites, whereas Gr-III samples are granodiorites (Fig. 2).

Gr-I samples display both equigranular, medium-grained texture (granodiorites and leucogranites), and inequigranular medium- to coarse-grained texture with pink poikilitic K-feldspars (monzogranites). Graphic textures are common in the most evolved Gr-I samples. Gr-II samples show equigranular, sometimes slightly inequigranular, medium- to coarse-

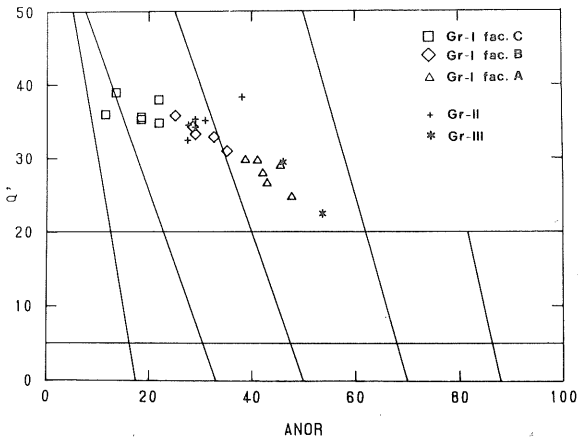

Fig. 2. Normative classification diagram (Streckeisen and Le Maitre, 1979) of the Punta Falcone granitic rocks.

TABLE 1

Representative plagioclase analyses from Gr-I, Gr-II, and Gr-III stocks; structural formula recalculated on the basis of 32 oxygens

	Gr-I fac. A		Gr-I fac. B		Gr-I fac. C		Gr-II		Gr-III		Gr-III	
	core*	rim	core	rim	core	rim	core	rim	core	rim	core	rim
SiO_2	59.00	62.90	58.69	61.11	58.46	62.46	60.12	64.41	54.26	58.76	59.90	62.47
TiO_2	0.05	0.00	0.01	0.00	0.01	0.00	0.00	0.00	0.03	0.00	0.01	0.00
Al_2O_3	26.41	23.90	25.63	24.27	26.72	24.12	25.77	21.99	28.64	25.73	25.80	24.14
FeO	0.12	0.11	0.11	0.09	0.06	0.10	0.02	0.17	0.13	0.13	0.11	0.12
CaO	7.58	4.83	7.20	5.85	7.71	5.03	7.15	3.23	10.60	7.29	7.13	4.99
Na_2O	6.94	8.46	7.07	8.06	6.94	8.44	7.45	9.71	5.30	6.99	7.26	8.54
K_2O	0.25	0.43	0.29	0.40	0.21	0.22	0.20	0.21	0.21	0.33	0.28	0.19
Total	100.35	100.63	99.00	99.78	100.11	100.37	100.71	99.72	99.17	99.23	100.49	100.45
Si	10.496	11.079	10.577	10.892	10.431	11.021	10.639	11.397	9.869	10.568	10.627	11.016
Al	5.538	4.955	5.445	5.099	5.619	5.016	5.375	4.586	6.140	5.455	5.395	5.018
Ti	0.007	0.000	0.001	0.000	0.001	0.000	0.000	0.000	0.004	0.000	0.001	0.000
Fe	0.000	0.006	0.000	0.010	0.000	0.000	0.000	0.017	0.000	0.000	0.000	0.000
Z	16.041	16.030	16.024	16.000	16.051	16.037	16.014	16.000	16.013	16.023	16.023	16.034
Fe	0.018	0.013	0.017	0.004	0.009	0.015	0.003	0.008	0.020	0.002	0.016	0.018
Ca	1.445	0.915	1.390	1.117	1.474	0.951	1.356	0.612	2.065	1.405	1.355	0.943
Na	2.394	2.880	2.470	2.785	2.401	2.887	2.556	3.331	1.869	2.437	2.497	2.920
K	0.057	0.090	0.067	0.091	0.048	0.050	0.045	0.047	0.049	0.076	0.063	0.043
X	3.913	3.919	3.944	3.997	3.931	3.902	3.960	3.999	4.003	3.938	3.932	3.923
Total	19.953	19.949	19.967	19.997	19.982	19.939	19.974	19.999	20.016	19.961	19.955	19.956
An (%)	37.09	23.39	35.40	27.97	37.57	24.46	34.26	15.34	51.85	35.86	34.61	24.14
Ab (%)	61.45	74.13	62.90	69.75	61.21	74.27	64.60	83.46	46.92	62.21	63.77	74.76
Or (%)	1.46	2.48	1.70	2.28	1.22	1.27	1.14	1.19	1.22	1.93	1.62	1.09

The complete sets of microprobe analyses of Tables I, II, III are available from the authors on request.
*Analysis used in the feedback system (see text).

grained textures. Gr-III samples are equigranular and medium-grained.

The mafic minerals of Gr-I and Gr-III comprise both biotite and hornblende, whereas Gr-II contains only biotite. The mafic minerals of Gr-I sometimes occur in clots. Common accessory phases are apatite, zircon, titanite and allanite. Accessory minerals show euhedral habits and are enclosed in plagioclase and mafic mineral phases. Secondary minerals are chlorite and magnetite derived from the alteration of mafic phases, and sericite derived from the alteration of feldspars.

Plagioclase shows euhedral and subhedral habits and it is normally zoned (Table 1). In all the facies of Gr-I, plagioclase has quite constant compositions both in cores (An_{37-31}) and rims (An_{28-20}) (Fig. 3). Plagioclase from Gr-II has mainly oligoclase compositions, with cores of An_{34-13}, and rims of An_{29-11} (Fig. 3). In contrast, plagioclase from Gr-III shows a range in composition decreasing from An_{51} to An_{28} (cores), and from An_{33} to An_{24} (rims) (Fig. 3).

Orthoclase exhibits an anhedral habit. In the monzogranites of Gr-I and Gr-II, it is poikilitic with respect to plagioclase and mafic minerals. It is always strongly perthitic and shows a restricted compositional range (Or_{85-97}) in all the stocks.

Hornblende occurs in euhedral crystals. According to the classification of Leake (1978), the amphiboles of Gr-I are magnesio-hornblendes, whereas those of Gr-III are magnesio-

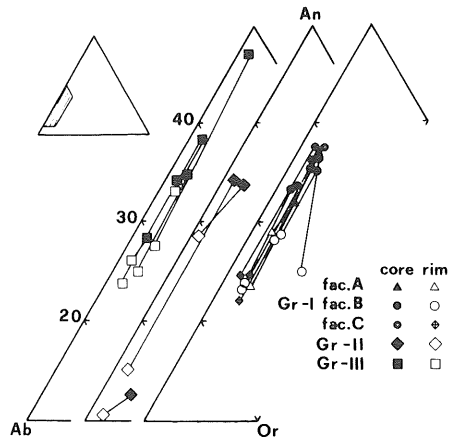

Fig. 3. Plagioclase compositions of the Punta Falcone granitic rocks. Core–rim tie lines are also shown.

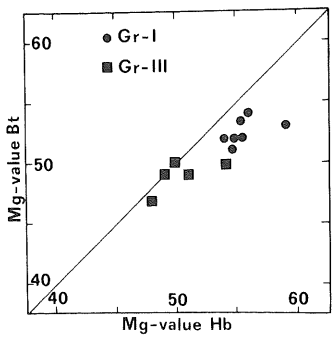

Fig. 4. Diagram of the Mg-values [$Mg/(Mg+Fe^{2+})$ mol%] for hornblende–biotite pairs of the Punta Falcone granitic rocks.

ferro-hornblendes. The hornblendes in the Gr-III stock are richer in Na_2O and TiO_2 and poorer in MgO than those of Gr-I (Table 2). In both Gr-I and Gr-III, the hornblendes have typical magmatic compositions in terms of their SiO_2, FeO, MgO, Na_2O, and K_2O contents (Gilbert, 1982). A plot of the Mg-value [$Mg/(Mg+Fe^{2+})$ mol%] for hornblende–biotite pairs from Gr-I and Gr-III (Fig. 4) shows that these minerals plot close to the 1:1 line, indicating crystallization under equilibrium conditions. Application of the empirical hornblende geobarometer of Hammarstrom and Zen (1986) yields pressures of crystallization of about 3–4 kbar for both Gr-I and Gr-III.

TABLE 2

Representative hornblende analyses from Gr-I and Gr-III stocks; structural formula recalculated on the basis of 13 cations exclusive of Ca, Na, K (Robinson et al., 1982)

	Gr-I fac. A		Gr-I fac. B		Gr-III	
	(*)					
SiO_2	44.12	46.49	45.12	45.04	42.94	43.77
TiO_2	1.21	0.98	1.02	0.80	1.59	1.47
Al_2O_3	8.48	6.72	8.10	8.09	9.05	8.55
Cr_2O_3	0.00	0.02	0.04	0.02	0.02	0.00
FeO	20.26	18.89	19.59	19.47	20.45	21.19
MnO	0.82	0.92	0.89	0.91	0.76	1.05
MgO	9.41	10.62	9.62	9.56	8.66	8.22
CaO	11.35	11.48	11.23	11.36	11.22	11.00
Na_2O	1.19	0.99	1.08	1.00	1.24	1.38
K_2O	1.01	0.69	0.92	0.90	1.05	1.02
Total	97.85	97.80	97.61	97.15	96.98	97.65
Si	6.616	6.902	6.747	6.769	6.531	6.631
Al	1.384	1.098	1.253	1.231	1.469	1.369
Z	8.000	8.000	8.000	8.000	8.000	8.000
Al	0.115	0.078	0.174	0.203	0.154	0.157
Fe^{3+}	0.809	0.732	0.758	0.722	0.723	0.704
Ti	0.136	0.109	0.115	0.090	0.182	0.167
Cr	0.000	0.002	0.005	0.002	0.002	0.000
Mg	2.103	2.350	2.144	2.141	1.963	1.856
Fe^{2+}	1.732	1.614	1.692	1.726	1.879	1.981
Mn	0.104	0.116	0.113	0.116	0.098	0.135
Y	5.000	5.000	5.000	5.000	5.000	5.000
Ca	1.824	1.826	1.799	1.829	1.829	1.786
Na	0.176	0.174	0.201	0.171	0.171	0.214
X	2.000	2.000	2.000	2.000	2.000	2.000
Na	0.170	0.111	0.112	0.121	0.194	0.191
K	0.193	0.131	0.176	0.173	0.204	0.197
W	0.363	0.242	0.288	0.293	0.398	0.388
Total	15.363	15.242	15.288	15.293	15.398	15.388
Mg#	54.83	59.28	55.88	55.37	51.09	48.36
char.	45.191	45.268	45.242	45.278	45.277	45.296

Fe^{3+} recalculated on the basis of charge balance.
(*): Analysis used in the feadback system (see text).

Biotite occurs as euhedral crystals and has a restricted range of composition in all the facies of Gr-I (Table 3). According to the classification of Deer et al. (1971), it is composed of about 25 mol% of each of the four biotite end members (Table 3). Biotite occurring in the

TABLE 3

Representative biotite analyses from Gr-I, Gr-II and Gr-III stocks; structural formula recalculated according to Dymek (1983)

	Gr-I			Gr-II	Gr-III
	fac.A (*)	fac.B	fac.C		
SiO_2	35.64	36.64	36.27	34.46	36.04
TiO_2	2.89	3.56	4.09	3.72	3.78
Al_2O_3	14.97	14.16	14.41	16.40	14.42
Cr_2O_3	0.00	0.00	0.00	0.02	0.02
FeO	21.92	22.29	20.61	23.62	22.05
MnO	0.52	0.59	0.78	0.88	0.45
MgO	10.41	10.26	10.37	7.04	9.60
CaO	0.02	0.04	0.06	0.02	0.07
K_2O	9.83	9.73	9.64	9.52	9.48
Total	96.20	94.27	96.23	95.77	95.91
Si	2.714	2.754	2.737	2.669	2.746
Al	1.286	1.246	1.263	1.331	1.254
Z	4.000	4.000	4.000	4.000	4.000
Al	0.058	0.009	0.019	0.166	0.041
Fe^{3+}	0.270	0.297	0.306	0.207	0.278
Ti	0.166	0.201	0.232	0.217	0.217
Cr	0.000	0.000	0.000	0.001	0.001
Mg	1.181	1.149	1.166	0.812	1.090
Fe^{2+}	1.126	1.104	0.995	1.322	1.127
Mn	0.034	0.038	0.050	0.058	0.029
Y	2.834	2.799	2.768	2.783	2.783
Ca	0.002	0.003	0.005	0.002	0.006
K	0.955	0.933	0.928	0.941	0.922
W	0.957	0.936	0.933	0.956	0.928
Total	7.791	7.735	7.701	7.739	7.711
Mg	51.19	50.99	53.97	38.05	49.17
char.	21.730	21.703	21.694	21.793	21.722
Easton.	29.28	25.09	28.39	25.19	24.98
Sider.	27.92	24.11	24.21	41.01	25.82
Annite	20.89	24.90	21.82	20.94	25.01
Phlog.	21.91	25.90	25.58	12.86	24.19

Fe^{3+} determined on the basis of charge balance.
(*): Analysis used in the feedback system (see text).

Gr-III stock has the same composition, whereas biotite of the Gr-II stock is poorer in Mg and richer in tetrahedral Al than that of Gr-I (Table 3). The Al_2O_3–FeO_{tot}–MgO diagram (Fig. 5A) shows that biotites of Gr-I and Gr-III fall in the field of biotites co-existing with amphibole (field I), whereas those of Gr-II lie in the field of biotites unaccompanied by other ferromagnesian minerals (field II), in agreement with petrographical data. The euhedral shape of the biotite crystals, and the correlation between the Mg-value of biotite–hornblende pairs (Fig. 4) support a magmatic origin for the biotites. On the Fe^{2+}–Fe^{3+}–Mg diagram (Fig. 5B), all biotites fall between the H–M and NiO–Ni buffers, though biotites of Gr-II suggest a slightly lower f_{O_2}.

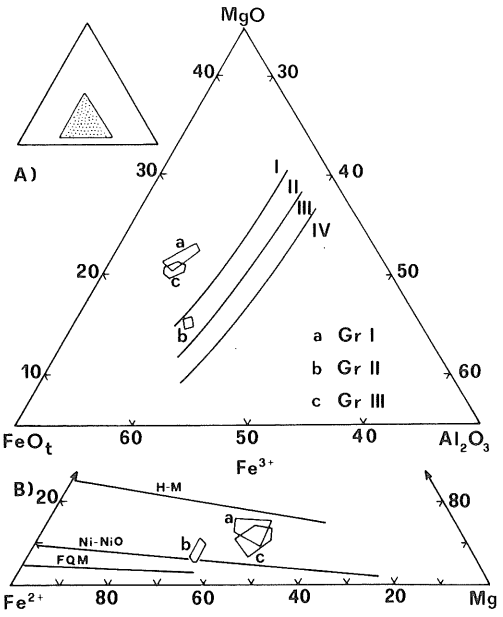

Fig. 5. A. Al_2O_3–FeO_{tot}–MgO diagram (De Albuquerque, 1973) of the biotites of the Punta Falcone granitic rocks. Field I: biotites co-existing with amphiboles; field II: biotites unaccompanied by other ferro-magnesian minerals; field III: biotites co-existing with muscovite; field IV: biotites co-existing with aluminosilicates.
B. Fe^{3+}–Fe^{2+}–Mg diagram (Wones et al., 1965) of the biotites of the Punta Falcone granitic rocks.

4. Geochemistry

Major- and trace-element analyses were carried out on 25 samples of the Punta Falcone granitic intrusions (Table 4); only two samples of Gr-III were analyzed owing to its small outcrop area (Fig. 1). The geochemical differ-

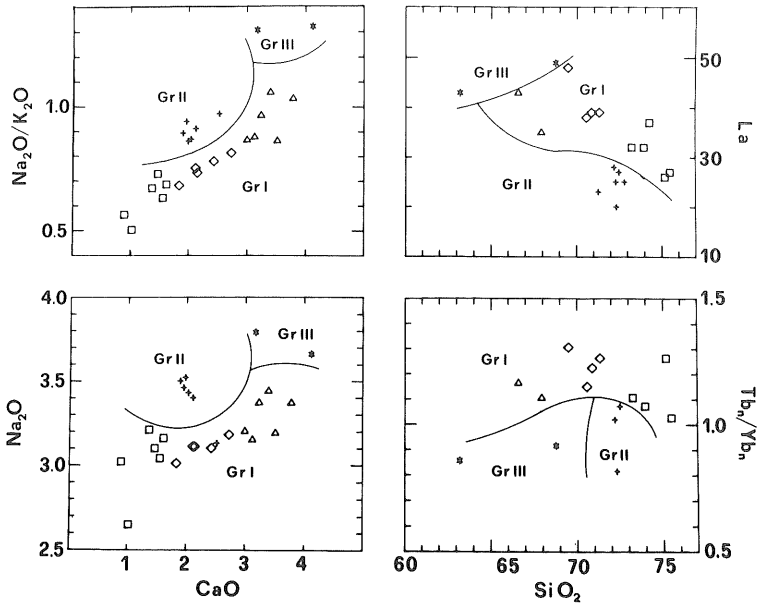

Fig. 6. Discriminant Harker diagrams for the Punta Falcone granitic stocks. Symbols as in Fig. 2.

ences among the three stocks are shown in the diagrams of Fig. 6. Samples from Gr-II and Gr-III have higher Na_2O contents and Na_2O/K_2O ratios, at the same CaO value, than Gr-I. The cause of the overlap of the Gr-II and Gr-I fields in the Na_2O versus CaO diagram is probably due to a slight alteration of sample SP 56. Gr-II samples show lower La contents than the other analyzed rocks. The $(Tb/Yb)_n$ ratio is near unity in the Gr-II and Gr-III samples, and slightly greater than unity in Gr-I samples, even though a partial overlap does exist between Gr-I samples belonging to facies C and Gr-II samples.

Some variation diagrams for Gr-I samples are reported in Fig. 7 using Sr as the differentiation index. SiO_2, K_2O, Rb, Th, and Ta are negatively correlated with Sr, whereas other major and trace elements show positive correlations. In all the diagrams, major and trace elements display straight-line trends with significant correlation coefficients (see caption to Fig. 7) at the 99% confidence level for most elements. Ta and HREE exhibit anomalous behaviour for some samples as discussed below.

All chondrite-normalized REE patterns (Fig. 8) exhibit fractionation of LREE and, as stated above, variable fractionation of HREE. Moreover, the Gr-I samples show a depletion in the REE content from the least to the most evolved sample, whereas the REE content of Gr-II is quite homogeneous and the REE content of Gr-III has increased significantly in sample SP 49 with respect to sample SP 83 (Table 4). Samples from Gr-I exhibit a marked increase in the negative Eu anomaly with differentiation; Gr-II samples display a moderate variation in the negative Eu anomaly, and the two Gr-III samples display both positive and negative Eu anomalies. Therefore, geochemical as well as petrographic features allow us to distinguish between the three granitic intrusions which outcrop in the Punta Falcone area.

In addition, geochemical variations also provide a tool for further discrimination within each stock: the Gr-I samples, which range from granodiorites to leucogranites, have the widest range of trace element variation (Figs. 6 and 7); Gr-II samples have relatively homogeneous compositions (Fig. 6); the two Gr-III samples, despite the restricted outcrop area, ex-

TABLE IV

Major (wt.%) and trace elements (ppm) whole-rock analyses of Gr-I, Gr-II and Gr-III

	Gr-I facies A						Gr-I facies B				
	SP 60	SP 59	SP 41	SP 146	SP 42	SP 88	SP 55	SP 45	SP 85	SP 58	SP 66
SiO_2	65.04	66.59	67.48	67.64	67.94	68.18	69.50	70.58	70.88	71.34	72.83
TiO_2	0.72	0.62	0.58	0.63	0.56	0.56	0.47	0.42	0.28	0.40	0.26
Al_2O_3	16.32	15.98	15.52	15.35	15.46	15.60	15.23	14.91	15.96	14.55	14.23
Fe_2O_3	1.50	1.46	1.41	2.45	1.39	1.33	0.85	0.71	0.94	1.14	1.18
FeO	3.03	2.55	2.60	1.99	2.47	2.40	2.20	2.08	1.40	1.70	1.04
MnO	0.06	0.08	0.08	0.09	0.08	0.07	0.06	0.06	0.06	0.06	0.05
MgO	1.64	1.33	1.30	1.15	1.27	1.18	0.91	0.85	0.48	0.61	0.52
CaO	3.78	3.51	3.23	3.39	3.12	2.99	2.72	2.42	2.14	2.11	1.83
Na_2O	3.37	3.19	3.37	3.44	3.15	3.20	3.18	3.10	3.11	3.11	3.01
K_2O	3.26	3.70	3.49	3.25	3.59	3.70	3.91	3.98	4.25	4.14	4.42
P_2O_5	0.17	0.14	0.15	0.11	0.10	0.15	0.14	0.09	0.05	0.11	0.05
LOI	1.12	0.86	0.80	0.52	0.87	0.63	0.82	0.80	0.45	0.73	0.59
ASI	1.05	1.04	1.05	1.02	1.07	1.09	1.08	1.10	1.18	1.10	1.10
Sc	–	14.0	–	–	10.2	–	9.0	8.5	5.6	7.5	–
Cr	–	20	–	–	17	–	10	15	–	–	–
Co	–	9.0	–	–	7.2	–	6.7	6.4	4.8	4.5	–
Rb	124	115	131	123	138	133	136	136	141	163	118
Sr	259	258	227	194	216	219	204	184	155	161	136
Y	49	65	42	25	44	37	32	30	28	40	22
Zr	260	254	229	242	221	237	202	183	168	197	156
Nb	19	21	19	16	14	17	14	15	13	17	14
Ba	882	1322	828	634	834	1065	1010	855	789	760	689
Hf	–	5.3	–	–	4.6	–	4.8	4.5	3.9	4.7	–
Ta	–	0.86	–	–	1.05	–	0.94	0.91	0.87	1.10	–
Th	–	7.7	–	–	11.6	–	11.6	11.6	13.4	14.7	–
La	–	43	–	–	35	–	48	38	39	39	–
Ce	–	84	–	–	57	–	93	71	74	81	–
Nd	–	27	–	–	31	–	44	33	24	29	–
Sm	–	6.3	–	–	7.0	–	6.0	5.2	4.2	5.4	–
Eu	–	1.50	–	–	1.10	–	1.30	1.10	0.90	0.95	–
Tb	–	0.77	–	–	0.72	–	0.80	0.62	0.66	0.65	–
Yb	–	2.70	–	–	2.66	–	2.50	2.20	2.20	2.10	–
Lu	–	0.40	–	–	0.41	–	0.41	0.34	0.38	0.30	–
Eu/Eu*		0.92			0.67		0.79	0.83	0.73	0.68	
Tb_n/Yb_n		1.16			1.10		1.31	1.15	1.22	1.26	
ΣREE		188			154		219	170	164	178	

ASI: $(Al_2O_3/(Na_2O+K_2O+CaO))$ mol%, corrected for apatite content.
–: not determined. Major elements (exclusive of FeO, MgO, Na_2O, P_2O_5 and LOI determined by wet chemical analyses) analyzed by X-ray fluorescence spectrometry (XRF) with full matrix correction after Franzini et al., 1972; Rb, Sr, Y, Zr, Nb, Ba by XRF after Kaye (1965); Sc, Cr, Co, Hf, Ta, Th, and REE by instrumental neutron activation analysis (INAA) (Poli et al., 1977). Values of La and Ce in brackets were determined by XRF.

hibit a significant chemical variation in major and trace elements (Fig. 6; Table 4).

Petrographical and geochemical data also suggest that all these intrusions can be classified as I-type granitoids, and support an origin by partial melting of igneous lower crustal material (Tommasini et al., in prep.). In fact, even though ASI (alumina saturation index) values point to a slightly peraluminous character (Table 4), the Na_2O and K_2O contents (Table 4) as well as the presence of hornblende (excluding the Gr-II samples) and titanite in all samples support the I-type character (see Chappell and White, 1974).

Gr-I facies C						Gr-II						Gr-III	
SP 87	SP 68	SP 78	SP 105	SP 106	SP 86	SP 157	SP 56	SP 40	SP 156	SP 158	SP 154	SP 83	SP 49
73.25	73.35	73.96	74.29	75.18	75.48	71.26	72.20	72.30	72.33	72.49	72.81	63.19	68.77
0.25	0.27	0.22	0.21	0.13	0.16	0.30	0.24	0.27	0.25	0.28	0.24	0.73	0.56
14.19	14.15	14.29	13.56	13.33	13.47	15.03	15.48	14.54	14.68	14.41	14.52	18.21	15.61
0.69	0.86	0.95	0.81	0.43	0.53	1.55	0.88	0.82	1.13	1.08	0.92	1.60	1.23
1.08	0.94	0.60	1.12	1.00	0.64	1.10	1.28	1.56	1.20	1.39	1.30	3.16	2.40
0.05	0.05	0.04	0.06	0.05	0.03	0.09	0.06	0.08	0.08	0.08	0.07	0.09	0.08
0.38	0.43	0.30	0.43	0.20	0.20	0.48	0.32	0.51	0.37	0.48	0.38	1.53	1.00
1.61	1.55	1.36	1.46	0.89	1.02	1.98	2.51	1.95	2.03	2.11	1.89	4.12	3.17
3.16	3.04	3.21	3.10	3.02	2.65	3.52	3.13	3.46	3.43	3.40	3.50	3.66	3.79
4.61	4.82	4.79	4.26	5.36	5.27	4.09	3.22	3.68	3.95	3.73	3.92	2.77	2.90
0.05	0.19	0.05	0.03	0.05	0.03	0.10	0.11	0.12	0.08	0.09	0.08	0.21	0.16
0.68	0.36	0.22	0.65	0.37	0.52	0.50	0.56	0.73	0.46	0.46	0.36	0.73	0.83
1.09	1.12	1.11	1.10	1.09	1.14	1.11	1.20	1.12	1.09	1.09	1.09	1.14	1.06
5.6	–	4.6	3.4	4.10	3.4	–	4.5	5.00	–	5.1	–	14.5	12.2
11	–	3	–	–	8	–	2	–	–	–	–	19	–
4.1	–	2.6	2.5	2.7	2.9	–	2.6	2.5	–	2.8	–	9.5	6.5
164	159	181	153	173	152	171	129	138	147	149	153	100	118
115	117	103	108	43	86	159	185	164	155	168	139	298	232
26	29	34	23	33	27	24	30	35	22	25	26	37	70
132	140	134	142	109	120	135	120	136	119	129	128	291	246
15	16	16	11	18	11	12	15	20	12	11	10	17	20
560	569	498	544	466	483	568	538	570	558	535	567	945	969
3.4	–	3.2	3.7	2.9	4.0	–	3.1	3.2	–	3.4	–	6.9	5.7
0.78	–	1.16	1.00	1.70	1.09	–	1.10	1.00	–	1.20	–	0.90	1.80
16.3	–	16.8	13.6	16.3	14.0	–	10.3	10.9	–	11.0	–	8.8	14.2
32	–	32	37	26	27	(23)	28	25	(20)	27	(25)	43	49
66	–	55	63	49	65	(43)	54	49	(43)	56	(56)	91	102
24	–	23	25	21	34	–	22	16.1	–	25	–	38	42
5.3	–	4.9	4.1	4.6	6.2	–	3.9	4.7	–	4.7	–	5.1	8.3
0.78	–	0.71	0.60	0.40	0.91	–	0.87	0.76	–	0.80	–	1.60	1.40
0.57	–	0.60	–	0.96	0.69	–	0.60	0.52	–	0.71	–	0.65	1.10
2.10	–	2.28	2.20	3.10	2.74	–	2.40	2.60	–	2.70	–	3.10	4.90
0.31	–	0.40	–	0.50	0.45	–	–	0.40	–	–	–	0.46	0.71
0.61		0.56	0.52	0.25	0.60		0.78	0.68		0.60		1.22	0.64
1.11		1.07	1.11	1.26	1.03		1.02	0.82		1.07		0.86	0.92
148		137	150	128	157		128	114		136		204	241

5. Discussion

The strongly perthitic nature of the K-feldspar and the hornblende geobarometer (Hammarstrom and Zen, 1986) indicate that the emplacement of these intrusions occurred at medium crustal levels (10–12 km). Furthermore, the biotite chemistry (Fig. 5B) suggests similar f_{O_2} conditions, between the H–M and NiO–Ni buffers, during the crystallization of each stock. Nevertheless, field observations, and petrographic, geochemical, and mineral chemistry data, indicate that the three granitic stocks underwent different evolutionary

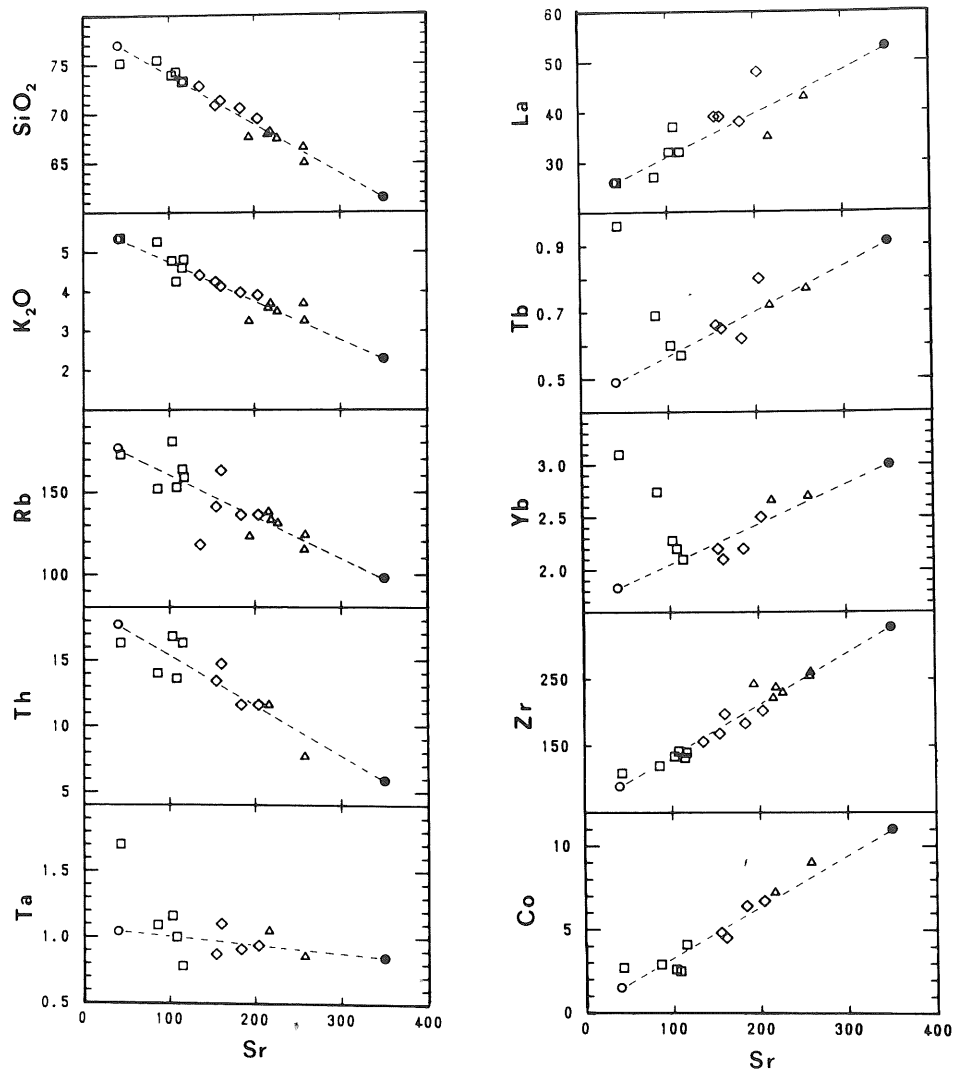

Fig. 7. Gr-I whole-rock variation diagrams for major and trace elements, plotted versus Sr abundances. Liquid (open circle) and solid (closed circle) end members are also shown (see text for explanation). Other symbols as in Fig. 2. Correlation coefficients (R) of the regression lines are (including elements not shown in figure): $SiO_2 = -0.97$; $TiO_2 = 0.96$; $Al_2O_3 = 0.91$; $FeO_{tot} = 0.94$; $MnO = 0.74$; $MgO = 0.96$; $CaO = 0.97$; $Na_2O = 0.96$; $K_2O = 0.92$; $P_2O_5 = 0.89$; $Sc = 0.94$; $Co = 0.96$; $Rb = -0.87$; $Y = 0.67$; $Zr = 0.97$; $Nb = 0.49$; $Ba = 0.86$; $Hf = 0.91$; $Ta = -0.33$; $Th = -0.88$; $La = 0.84$; $Ce = 0.67$; $Nd = 0.72$; $Sm = 0.55$; $Eu = 0.93$; $Tb = 0.84$; $Yb = 0.80$; $Lu = 0.74$. Samples SP106 and SP86 have been excluded from the regression line calculation of Tb, Yb, and Lu; sample SP 106 has also been excluded from the regression line calculation of Ta (see text for explanation).

processes.

The Gr-II stock exhibits a fairly homogeneous composition in terms of both the whole-rock chemical analyses and mineral chemistry data, indicating that it may represent a single magmatic batch which did not undergo significant differentiation during its cooling history.

In contrast, both mineral chemistry and geochemical data (Table 4) suggest that the variations between the two Gr-III samples are probably due to a fractional crystallization process, with separation mainly of plagioclase

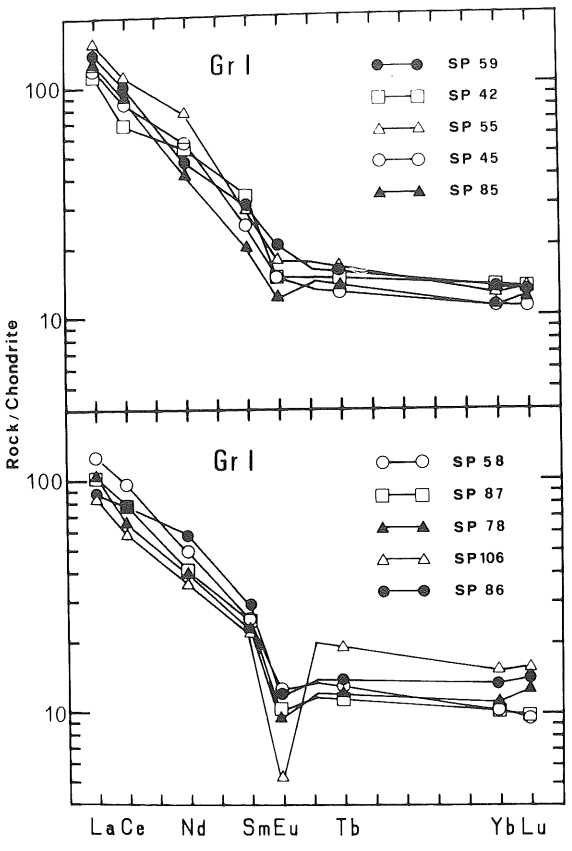

Fig. 8. Chondrite-normalized (Haskin et al., 1966) REE patterns of the Punta Falcone granitic rocks.

and subordinately of hornblende, biotite, and accessory amounts of zircon.

A more detailed discussion of the differentiation history of the Gr-II and Gr-III stocks is beyond the aim of this paper, inasmuch as it concerns the study of the more complex differentiation history of the Gr-I stock.

5.1. Constraints on Gr-I differentiation

Any model attempting to represent the processes which operated during the differentiation of the Gr-I stock must account for the following geological, petrographic, and geochemical features: (i) the three Gr-I facies exhibit transitional contacts; (ii) mineral chemistry data indicate that hydromorphic mineralogical phases (plagioclase cores, biotite, hornblende) have constant compositions in all three facies of Gr-I (Tables 1–3), and they show no evidence of resorption or reaction rims; (iii) in bivariate diagrams, all elements display straight line trends with significant correlation coefficients (Fig. 7).

Accordingly, the following processes were considered in order to explain the differentiation of Gr-I stock: (1) Rayleigh fractional crystallization; (2) mixing between different magmas; (3) restite unmixing; (4) unmixing within a single magmatic batch.

The hypothesis of a simple fractional crystallization process is plausible on the basis of the transitional contacts among the Gr-I facies. However, the question arises how to get straight-line trends in all bivariate diagrams, in particular for the trace elements (Fig. 7). Theoretically, Rayleigh fractional crystallization can produce straight-line bivariate diagrams only if two elements have the same value for the bulk distribution coefficient, and provided there is no change in the fractionating mineral assemblage. In practice, it may be arguable to distinguish between a straight-line and an exponential trend if the degree of crystallization is not very large (e.g. 20–30%), and if the bulk distribution coefficients of trace-element pairs are similar. As regards the Gr-I stock, there are several constraints which rule out fractional crystallization as the dominant process responsible for its differentiation:

(A) The condition that the bulk distribution coefficients of trace-element pairs are similar is not always satisfied, e.g. Rb and Sr behave as incompatible, and compatible elements, respectively (Fig. 7); and hence they have very different bulk distribution coefficients.

(B) Calculations using XLFRAC (Stormer and Nicholls, 1978) indicate that a large degree of solid segregation (about 50%) is necessary to pass from granodiorites to leucogranites.

(C) It is unlikely that the fractionating mineral assemblage did not change during the frac-

tional crystallization process, e.g. K-feldspar started to crystallize during the sequence of evolution from granodiorite to leucogranite.

(D) In a regime of a changing liquid composition (from granodiorite to monzogranite and leucogranite), the compositions of the coexisting liquids and solids must change sympathetically: how is it then possible for the plagioclase cores, biotite, and hornblende to have the same composition in all the three Gr-I facies (Tables 1–3)? The euhedral grain shape of the above phases, with evidence of neither resorption nor reaction rims, suggests that they crystallized in equilibrium with the liquid, and excludes the possibility of them representing early-stage minerals entrained during segregation of the successive liquids from the parental granodioritic magma.

On the other hand, the straight-line trends in the bivariate diagrams (Fig. 7) may also be the result of a mixing process.

The process of mixing of different magmas (i.e. a leucogranite and a granodiorite) can account for the geochemical variations of Gr-I samples. However, a mixing process between a crystal-mush (i.e. granodiorite) and a crystal-free magma (i.e. leucogranite) must be assumed to explain the identical compositions of the main mineralogical phases. Accordingly, disequilibrium textures (e.g. Hibbard, 1981) should occur in the Gr-I samples. The absence of such textures rules out the operation of such a mixing process. In addition, the high viscosity of felsic magmas prevents large-scale mixing processes such as would be needed to account for the differentiation of the Gr-I stock.

The restite unmixing model has recently been the subject of some controversy (e.g. Chappell et al., 1987; Wall et al., 1987). Questions arise especially concerning the mineralogical, textural and chemical criteria for the recognition of restite components, and the possibility that restite is entrained during segregation of the melt from the residual source rock. As regards the evolution of the Gr-I stock, restite unmixing does not seem to have played a dominant role: plagioclase cores, hornblendes, and biotites have euhedral shapes, whereas restite phases should show anhedral and resorbed grain shapes. In addition, hornblende and biotite exhibit magmatic compositions, and have features indicating an almost contemporary crystallization under equilibrium conditions (Fig. 4). Plagioclase zoning with constant core compositions in the three Gr-I facies may be taken as evidence for a restite origin; however, their anorthite contents (37–31%) are not as calcic as inferred by proponents of the restite model (ca. An_{80}, Chappell et al., 1987). In conclusion, mineralogical and textural evidence suggests that restite incorporation is not the major factor controlling the chemical variation of the Gr-I stock.

Instead, an unmixing process within a single magmatic batch can account for all the observed chemical and petrographical variations of Gr-I stock. The proposed evolutionary model consists of two main stages: (1) the Gr-I parental magma undergoes an in-situ fractional crystallization process developing a solid and a liquid phase, represented by early-crystallized minerals and residual liquid, respectively; (2) the relative proportions of the solid and liquid phases in the magma, by then a mush, are modified by a filter pressing process, which squeezes the liquid inward to the core of the intrusion (see below for a more detailed discussion of this physical process). Accordingly, the model accounts for the occurrence of transitional contacts among Gr-I facies as well as for the constant composition of plagioclase cores, biotites, and hornblendes (solid phase) in all the Gr-I facies, inasmuch as each sample represents a cumulus–intercumulus mixture between various proportions of solid and liquid phases.

5.2. The Gr-I unmixing model

In every mixing model, it is crucial to identify the chemical composition of the end members. Our strategy has been to determine the Sr

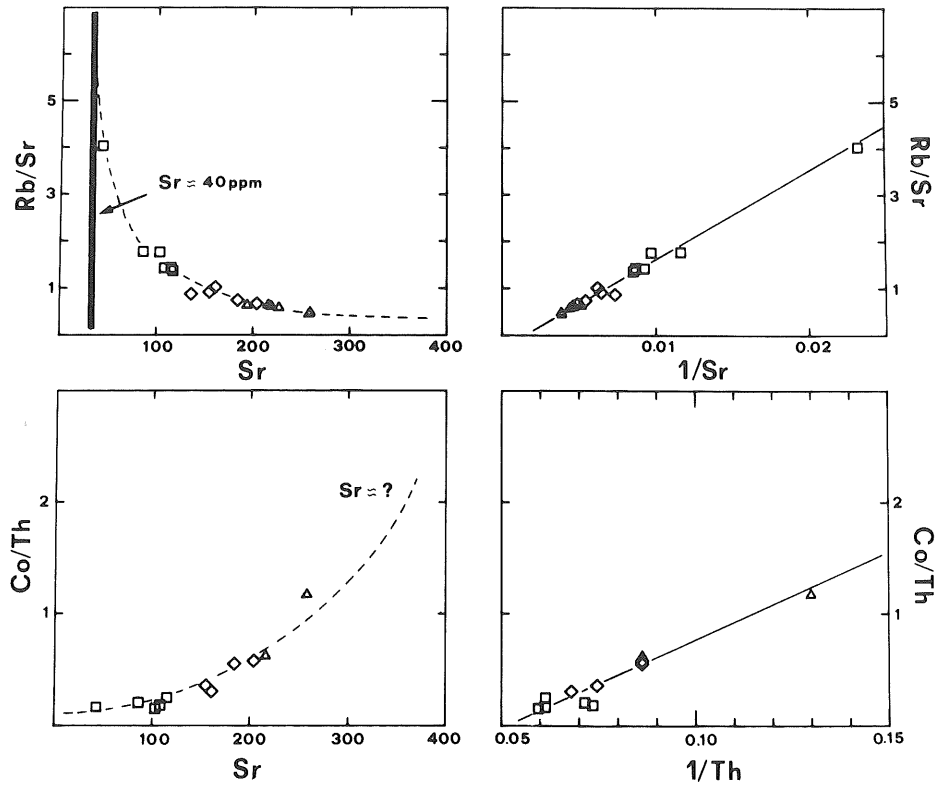

Fig. 9. Diagrams of trace- element ratios versus trace- element content and companion plots of the Gr-I rocks. Hyperbolic and straight-line trends are also indicated. Symbols as in Fig. 2.

concentration in both the solid and liquid end members, and to use bivariate diagrams with Sr as differentiation index (Fig. 7), to determine the concentrations of other elements (Table 6).

In agreement with a simple two end member mixing model (Langmuir et al., 1978), plots of trace element ratios versus trace element contents, and their companion diagrams (Fig. 9), display hyperbolic, and straight-line trends, respectively. Such diagrams also allow the concentration of an element in the end members to be determined from the asymptotes to the hyperbola, provided the radius of curvature of the hyperbola is not very large. From plots of incompatible/compatible element ratios versus Sr (e.g. Rb/Sr vs. Sr, Fig. 9), it was, thus, determined that 40 ppm is a plausible value for the Sr concentration in the liquid end member (C_l^{Sr}). In contrast, the Sr concentration in the solid end member (C_s^{Sr}) was determined using a *feedback system*, inasmuch as it cannot be accurately defined from plots of compatible/incompatible element ratios versus Sr (e.g. Co/Th vs. Sr, Fig. 9), owing to the large radius of curvature of the hyperbola.

The main steps of the "feedback system" are illustrated in the flow sheet of Fig. 10. Once a provisional bulk chemical composition of the solid end member has been determined (Steps I and II), an iterative mixing program based on major elements, is used to calculate its modal composition (weight%, Step III). The chemical composition of the solid end member (Step II) and representative analyses of the early-crystallized minerals (Tables 1–3), are used as entry data (quartz is assumed to be 100% SiO_2). In Step IV, the bulk distribution coefficients (D) of a set of trace elements are calculated using the modal composition of the

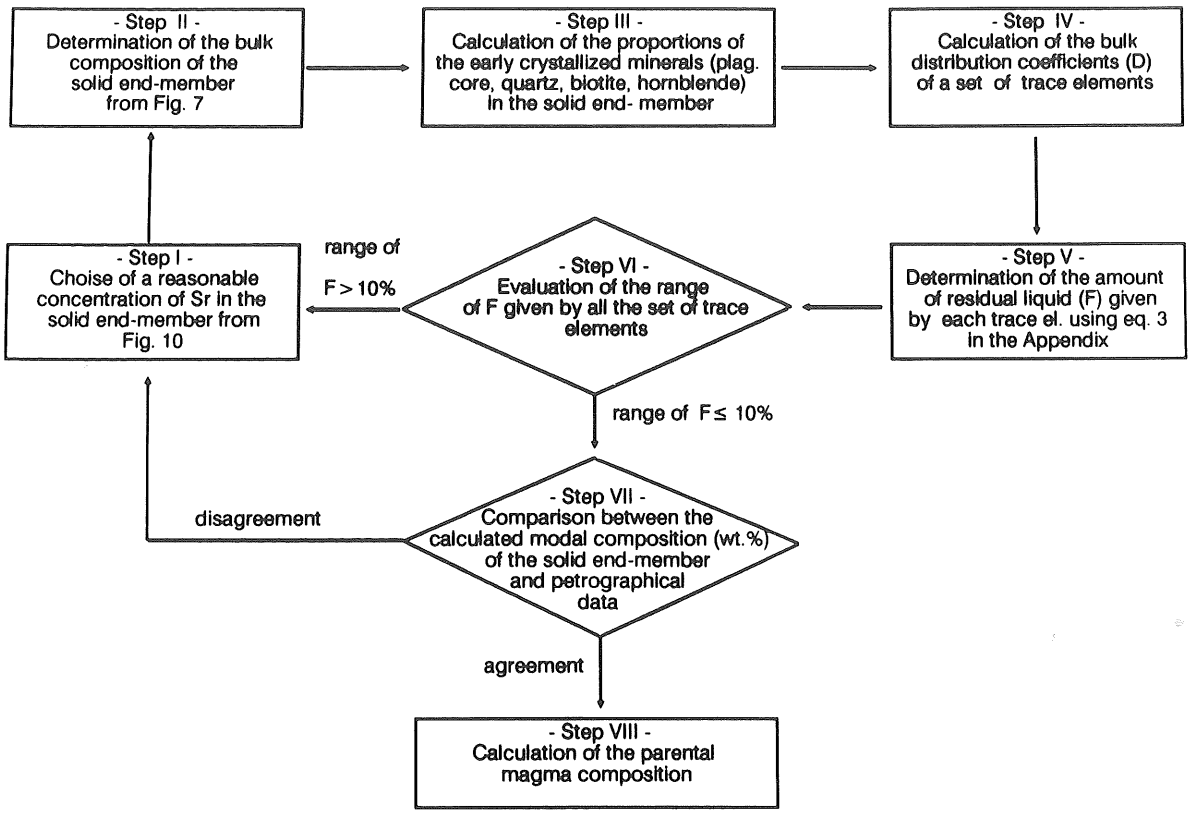

Fig. 10. Schematic flow sheet illustrating the "feedback system" employed in the calculation of the bulk chemical composition of the solid end member (see text for explanation). Distribution coefficients used in Step IV are reported in the Appendix (Table A-1).

solid end member (Step III) and by adding provisional amounts of accessory phases (apatite, zircon, titanite, and allanite). Accordingly, using the provisionally calculated D values, the amount of residual liquid (F) is determined for each trace element by solving eq. A-3 in the Appendix. The range of F given by all trace elements is then minimized by changing the amounts of the accessory phases, in accordance with estimates made on the basis of petrographic data. At this point, two conditions must be satisfied in order to exit from the iterative cycle: (i) the range of F given by all trace elements must be as narrow as possible, say less than 10% (Step VI); (ii) the calculated modal composition of the solid end member must be in agreement with petrographic data (Step VII). If just one, of these two conditions is not satisfied, the iterative cycle is repeated choosing another provisional Sr concentration for the solid end member (Step I). If, instead, both conditions are satisfied, the composition of the parental magma is calculated using eq. A-4 in the Appendix, and the plots of Fig. 7 (Step VIII).

In Table 5, the results of three provisional values of C_s^{Sr} (300, 350, 400 ppm) are reported as examples of the computed "feedback system". The value of $C_s^{Sr}=300$ ppm was rejected because the range of F given by the trace elements (Fig. 11A) is very large (20%–90%, Step VI of Fig. 10), and because the modal composition of the solid end member is not in agreement with petrographic data (hornblende is absent from the calculated mode, Step VII of Fig. 10). The value of $C_s^{Sr}=400$ ppm

TABLE 5

Major element compositions of three provisional solid end members

C_s^{Sr} (ppm)	300		350		400	
	A	B	A	B	A	B
SiO_2	63.98	64.15	61.49	61.49	58.99	58.99
TiO_2	0.78	0.82	0.92	0.81	1.06	0.80
Al_2O_3	16.66	16.10	17.00	16.62	18.05	17.38
FeO_t	4.88	5.01	5.68	5.80	6.49	6.31
MnO	0.09	0.13	0.10	0.16	0.10	0.20
MgO	1.72	2.27	2.05	2.64	2.38	2.88
CaO	4.24	4.03	4.95	4.92	5.66	5.63
Na_2O	3.35	3.68	3.42	3.85	3.47	4.09
K_2O	2.87	2.29	2.30	2.09	1.75	1.97
Sum of squares of residuals	1.1773		0.7525		0.9120	
pl [a]	53.1		54.4		57.0	
qz [a]	24.7		19.2		13.9	
bt [a]	22.2		19.4		17.6	
hb [a]	0.0		7.0		11.5	

[a] Computed modal compositions (wt.%) of the three provisional solid end members (pl = plagioclase; qz = quartz; bt = biotite; hb = hornblende)
(A) inferred from the bivariate plots of Fig. 7 according to the three values of C_s^{Sr}; (B) calculated with the mixing program using representative mineral analyses of Gr-I (labelled with "*" in Tables I, II, III)

was rejected because the range of F given by trace elements (Fig. 11C) is again very large (30%–90%). The best result was obtained for the value $C_s^{Sr} = 350$ ppm: the calculated modal composition of the solid end member agrees with the petrographic data, and the range of F given by the trace elements (Fig. 11B) is very narrow (65%–70%). Accordingly, the compositional range of the Gr-I parental magma was calculated (Table 6) on the basis of a 30–35% in-situ fractional crystallization involving the production of the solid and liquid phases (Step VIII of Fig. 10).

It is noteworthy that calculations using provisional Sr contents higher and lower than 350 ppm in the solid end member do not satisfy the conditions of Step VI and/or Step VII; therefore, the "feedback system" employed represents a self-consistent tool to determine the bulk composition of the solid end member.

Although the geochemical constraints are in good agreement with the proposed model, some samples scatter around the linear regression lines (Fig. 7). This scatter may be due to small-scale heterogeneities, both physical and mineralogical. Physical factors such as local variations in the degree of filter pressing, and mineralogical factors such as differences in sizes, shapes, and densities of minerals can complicate a perfect two end member mixing process. However, local variabilities in the unmixing cannot be invoked for the significantly higher contents in HREE and Ta of samples SP 86 and SP 106 (Fig. 7). High enrichment factors for HREE and high field strength elements (HFSE) are very common in the final stages of the crystallization of granitic melts (e.g. Mineyev, 1963; Taylor et al., 1981; Mittlefehldt and Miller, 1983; Poli et al., 1989). In the Gr-I samples, a further crystal–liquid fractionation process, or the escape of a late fluid phase from the Gr-I magma cannot explain these "anomalous" enrichments of Ta and HREE which are not accompanied by sympathetic variations of other trace elements. A possible explanation might be found in an increase in volatile activity (B, Cl, F, OH), which inhibits the crystallization of HREE and HFSE-consuming accessory phases (London et al., 1989) and allows the enrichment of HREE and HFSE in the residual melt.

Finally, we wish to emphasize the physical process responsible for the differentiation of the Gr-I stock. The main stages are illustrated in the schematic cartoon of Fig. 12: (i) the Gr-I parental magma undergoes a 30–35% in-situ fractional crystallization process which proceeds inwards from the walls developing a solid (early crystallized minerals), and a liquid (residual liquid) phase; (ii) the proportions of the two phases are then modified by filter pressing due to volume shrinkage during magma cooling, and/or to tectonic forces still acting on the environs of magma emplacement. Accordingly, the three Gr-I facies (Fig. 1) result from

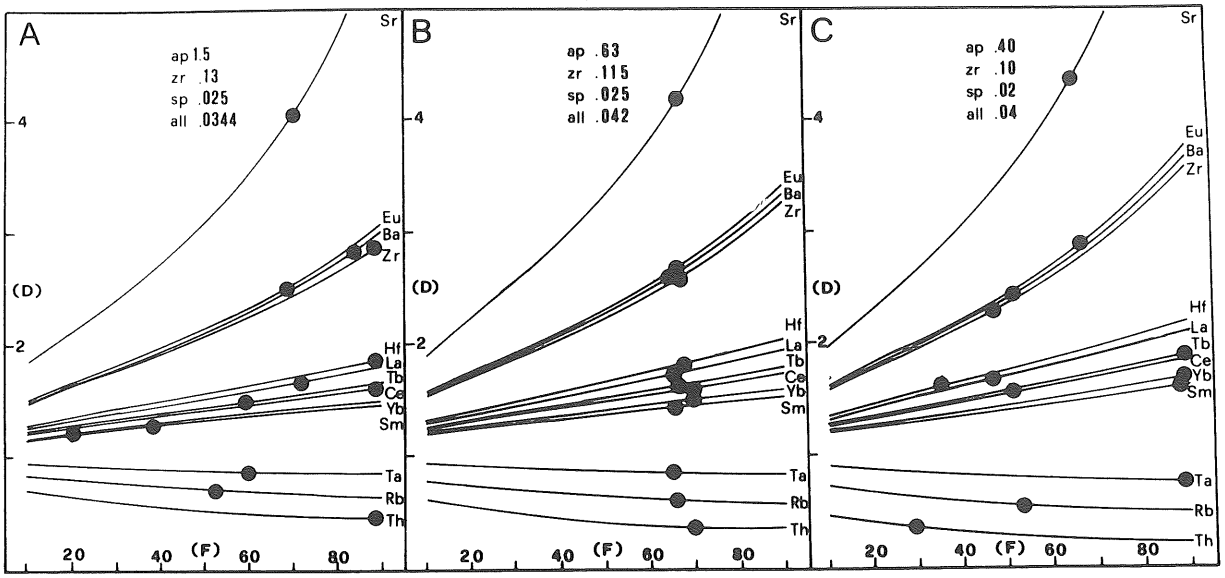

Fig. 11. Diagrams showing variations in the bulk distribution coefficient (D) for various trace elements as a function of the amount of residual liquid (solid lines, calculated from eq. A-3 in the Appendix). (A) $C_s^{Sr}=300$ ppm; (B) $C_s^{Sr}=350$ ppm; (C) $C_s^{Sr}=400$ ppm. Solid circles: calculated D_s using the different modal compositions of the three solid end-members (Table 6). The percentages (wt.%) of accessory phases are also reported in the figure.

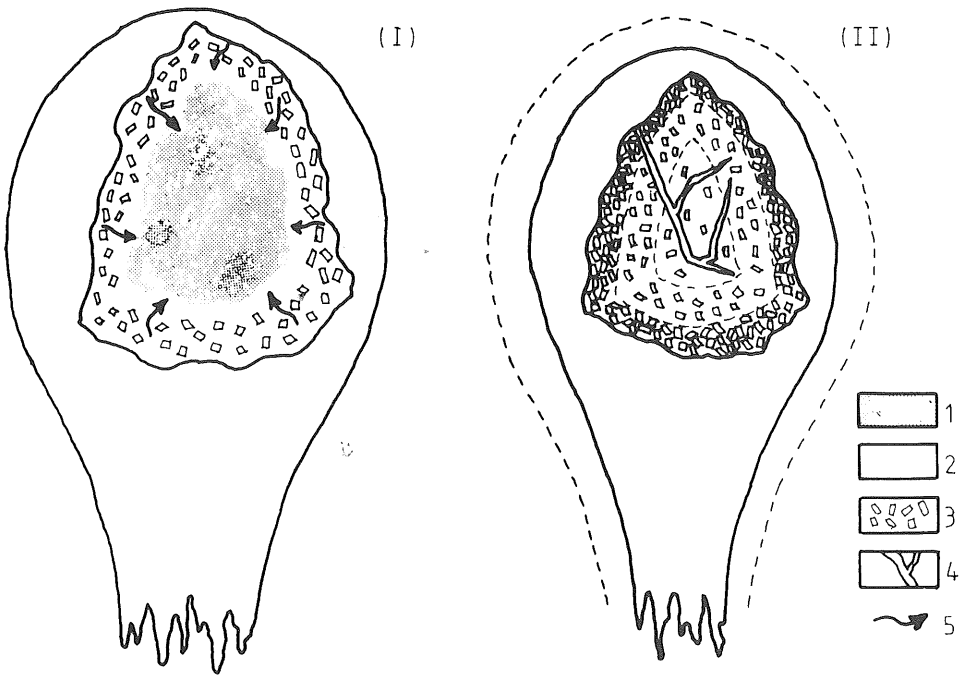

Fig. 12. Schematic cartoon illustrating the two-stage model proposed for the differentiation of the Gr-I stock (see text): *1*=parental granitic magma; *2*=residual liquid (liquid end member); *3*=early crystallized minerals (solid end member); *4*=aplitic dikes; *5*=direction of movement of the residual liquid.

TABLE 6

Whole-rock composition of the solid and liquid phases of the Gr-I stock, and compositional range of the Gr-I parental magma for different amounts of residual liquid (F)

	C_s	C_l	F (%)	
			65	70
SiO_2	61.49	76.99	71.59	72.34
TiO_2	0.92	0.04	0.35	0.30
Al_2O_3	17.00	13.15	14.60	14.40
FeO_t	5.68	0.69	2.43	2.19
MnO	0.10	0.04	0.06	0.06
MgO	2.05	0.01	0.72	0.62
CaO	4.95	0.54	2.08	1.86
Na_2O	3.42	3.00	3.14	3.12
K_2O	2.30	5.34	4.46	4.28
P_2O_5	0.21	0.01	0.08	0.07
Rb	98	177	149	153
Sr	350	40	148	133
Ba	1348	356	703	653
Zr	327	89	172	160
Th	5.9	17.7	13.5	14.0
Ta	0.85	1.04	0.98	1.0
Hf	6.3	2.9	4.1	3.9
La	53	26	36	34
Ce	97	54	69	66
Sm	6.9	4.4	5.2	5.1
Eu	1.83	0.47	0.94	0.88
Tb	0.91	0.49	0.64	0.62
Yb	3.00	1.83	2.24	2.18

an unmixing process within a single batch of magma.

Filter pressing by means of volume shrinkage can play an important role in the differentiation of granitic magmas. Simple calculations, based on density differences (using values at 1 atm) between an acid magma (ca. 2.2 g/cm^3) and a granitic rock (ca. 2.7 g/cm^3) yield a decrease of about 20% in the magma volume when it is completely solidified, thus allowing the migration of the residual liquid inward to the core of the intrusion.

6. Conclusions

In this paper, the complex differentiation history of a granitic stock (Gr-I) which outcrops in the Punta Falcone area has been studied, and a model for the evolution of granitic magmas by an unmixing process within a single magmatic batch has been proposed.

Fractional crystallization and restite unmixing processes have been considered, but they do not seem to be the dominant mechanisms which produced the geochemical variations of the Gr-I stock. Instead, whole-rock geochemistry and mineral chemistry data suggest that Gr-I differentiation can be quantitatively accounted for by a two-stage model. In the first stage, a 30–35% in-situ fractional crystallization occurred in the parental magma, producing a solid (early-crystallized minerals) and a liquid (residual liquid) phase, while subsequently, in the second stage, the proportions of these two phases were modified by a filter pressing segregation mechanism; therefore, each sample represents a cumulus–intercumulus mixture between the liquid and solid phases developed in stage I. The bulk chemical compositions of these phases have been determined using simple mixing diagrams, and a self-consistent "feedback system" of calculation, respectively. Filter pressing is the driving mechanism which favours the migration of the liquid towards the core of the intrusion, and results in the formation of the roughly concentric normal zoning of the Gr-I stock.

Acknowledgements

We would like to extend our special thanks to Prof. A. Peccerillo for his critical comments. Thanks are also due to Prof. D.B. Clarke, and Prof. J.A. Pearce for their reviews, which greatly improved the manuscript. Prof. P. Manetti, Prof. C. Garbarino, Dr. S. Conticelli, Dr. L. Francalanci and Mrs. L. Todaro are acknowledged for their help given during field and laboratory work. Major- and trace-element analyses were carried out at the "CNR-C.S. per la Mineralogia e Geochimica dei Sedimenti di Firenze", whereas microprobe analyses were carried out at the "Istituto di

Giacimenti Minerari di Cagliari". This work was supported by M.U.R.S.T. Grants 40% and 60%.

Appendix

Equations employed in the geochemical calculations (Allègre and Minster, 1978). Given:

$$C_l = C_{oF}^{(D-1)} \quad \text{(A-1)}$$

and:

$$C_s = \frac{C_o(1-F^D)}{1-F} \quad \text{(A-2)}$$

it follow that:

$$D = \frac{-\log[1 + C_s/C_l(F^{-1}-1)]}{\log F} \quad \text{(A-3)}$$

and:

$$C_o = C_l F^{(1-D)} \quad \text{(A-4)}$$

where C_o, C_l and C_s are the concentrations of a trace element in the parental magma, in the residual magma, and in the bulk separated solid fraction, respectively; F is the liquid fraction remaining after the fractionation process, and D is the bulk distribution coefficient of the fractionated assemblage.

TABLE A-1

Crystal liquid partition coefficients employed in the computed fractional crystallization exercise

	pl	bt	hb	ap	zr	tit	al
Rb	0.04	3.0	0.01	0.0	0.0	0.0	0.0
Sr	7.6	0.13	0.02	0.0	.0	0.0	0.0
Ba	0.81	10.8	0.42	0.0	0.0	0.0	0 .0
Zr	0.26	0.65	0.0	0.64	2000	0.0	0.0
Hf	0.2	0.36	0.0	0.73	1400	29	28
Th	0.01	0.24	0.29	0.0	91.2	56	420
Ta	0.04	1.0	0.33	0.0	54.8	2200	4.4
La	0.46	0.30	0.90	25.0	3.11	19.2	2827
Ce	0.28	0.32	1.52	34.7	3.49	33.6	2494
Sm	0.16	0.26	7.77	62.8	4.72	352	756
Eu	3.6	0.24	5.14	30.4	4.23	189	100
Tb	0.13	0.28	11.5	78.0	35.1	218	235
Yb	0.07	0.30	8.38	27.6	516	105	24.5

(pl = plagioclase; bt = biotite; hb = hornblende; ap = apatite; zr = zircon; tit = titanite; al = allanite). Kd for quartz are assumed for all elements equal to zero.

Source of data: Arth and Hanson, 1975; Crecraft et al., 1981; Fourcade and Allègre, 1981; Fujimaki, 1986; Hellman et al., 1979; Mahood and Hildreth, 1983; Rose et al., 1979; Verneries et al., 1977.

References

Allègre, C.J. and Minster, J.F., 1978. Quantitative models of trace element behaviour in magmatic processes. Earth Planet. Sci. Lett., 38: 1–25.

Arth, J.G. and Hanson, G.N., 1975. Geochemistry and origin of the early Precambrian crust of north eastern Minnesota. Geochim. Cosmochim. Acta, 39: 325–343.

Bralia, A., Ghezzo, C., Guasparri, G. and Sabatini, G., 1982. Aspetti genetici del Batolite Sardo–Corso. Rend. Soc. Ital. Mineral. Petrol., 38: 701–764.

Chappell, B.W. and White, A.J.R., 1974. Two contrasting granite types. Pac. Geol., 8: 173–174.

Chappel, B.W., White, A.J.R. and Wyborn, D., 1987. The importance of residual source material (restite) in granite petrogenesis. J. Petrol., 28: 1111–1138.

Crecraft, H.R., Nash, W.P. and Evans, S.H., 1981. Late Cenozoic volcanism at Twin Peaks, Utah: geology and petrology. J. Geophys. Res., 86: 10303–10320.

DeAlbuquerque, C.A.R., 1973. Geochemistry of biotites from granitic rocks, Northern Portugal. Geochim. Cosmochim. Acta, 37: 1779–1802.

Deer, W.A., Howie, R.A. and Zussman, J., 1971. An Introduction to the Rock-Forming Minerals. Longmans, London, 528 pp.

Dymek, R.F., 1983. Titanium, aluminum and interlayer cation substitutions in biotite from high-grade gneisses, West Greenland. Am. Mineral., 68: 880–899.

Fourcade, S. and Allègre, C.J., 1981. Trace element behaviour in granite genesis: a case study the calc-alkaline plutonic association from the Querigut Complex (Pyrénées, France). Contrib. Mineral. Petrol., 76: 177–195.

Franzini, M. and Leoni, L., 1972. A full matrix correction in X-ray fluorescence analysis of rock samples. Atti Soc. Toscana Sci. Nat., Ser. A, 79: 7–22.

Fujimaki, H., 1986. Partition coefficients of Hf, Zr and REE between zircon, apatite and liquid. Contrib. Mineral. Petrol., 94: 42–45.

Ghezzo, C. and Orsini, J.B., 1982. Lineamenti strutturali e composizionali del batolite ercinico sardo–corso in Sardegna. In: L. Carmignani, T. Cocozza, C. Ghezzo, P.C. Pertusati and C.A. Ricci (Editors), Guida alla Geologia del Paleozoico Sardo. Soc. Geol. Ital., pp. 88–102.

Gilbert, M.C., 1982. Brief overview of igneous amphiboles. In: D.R. Veblen and P.H. Ribbe (Editors) Reviews in Mineralogy, Amphiboles: Petrology and Experimental Phase Relations. Mineral. Soc. Am., 9B: 371–390.

Hammarstrom, J.M. and Zen, E., 1986. Aluminum in hornblende: an empirical igneous geobarometer. Am. Mineral., 71: 1297–1313.

Haskin, L.A., Frey, R.A., Schmitt, R.A. and Smith, R.H., 1966. Meteoric, solar and terrestrial abundances of the rare earths. Phys. Chem. Earth, 7: 167–321.

Hellman, P.L. and Green, T.H., 1979. The role of sphene as an accessory phase in the high pressure partial melting of hydrous mafic composition. Earth Planet. Sci. Lett., 42: 191–201.

Hibbard, M.J., 1981. The magma mixing origin of mantled feldspars. Contrib. Mineral. Petrol., 76: 158–170.

Hildreth, E.W., 1979. The Bishop Tuff: evidence for the origin of zoned magma chambers. In: C.E Chapin and W.E. Elston (Editors), Ash Flow Tuff. Geol. Soc. Am. Spec. Pap., 180: 43–72.

Hildreth, E.W., 1981. Gradients in silicic magma chambers: implication for lithospheric magmatism. J. Geophys. Res., 86: 10153–10192.

Kaye, M.J., 1965. X-ray fluorescence determinations of several trace elements in some standard geochemical samples. Geochim. Cosmochim. Acta, 29: 139–142.

Langmuir, C.H., Vocke, R.D. and Hanson, G.N., 1978. A general mixing equation with applications to Icelandic Basalts. Earth Planet. Sci. Lett., 37: 380–392.

Leake, B.E., 1978. Nomenclature of amphiboles. Am. Mineral., 63: 1023–1052.

London, D., Morgan, G.B. and Hervig, R.L., 1989. Vapor-undersaturated experiments with Macusani glass+H_2O at 200 MPa, and the internal differentiation of granitic pegmatites. Contrib. Mineral. Petrol., 102: 1–17.

Mahood, G. and Hildreth, E.W, 1983. Large partition coefficients for trace elements in high-silica rhyolites. Geochim. Cosmochim. Acta, 47: 11–30.

McCarty, T.S. and Fripp, R.E.P., 1978a. The crystallization of a granitic magma as revealed by trace element abundances. J. Geol., 88: 211– 224.

McCarty, T.S. and Hasty, R.A., 1976. Trace element distribution patterns and their relationship to the crystallization of granitic melts. Geochim. Cosmochim. Acta, 40: 1351–1358.

McCarty, T.S. and Robb, L.J., 1978b. On the relationship between cumulus mineralogy and trace and alkali element chemistry in an Archean granite from the Barbeton region, South Africa. Geochim. Cosmochim. Acta, 42: 21–26.

Michael, P.J., 1984. Chemical differentiation of the Cordillera Paine granite (Southern Chile) by in situ fractional crystallization. Contrib. Mineral. Petrol., 87: 179–195.

Mineyev, D.A., 1963. Geochemical differentiation of the rare earth. Geokhimiya, 12: 1082–1100.

Mittlefehldt, D.W. and Miller, C.F., 1983. Geochemistry of the Sweetwater Pluton, California: implications for "anomalous" trace elements behaviour during differentiation of felsic magmas. Geochim. Cosmochim. Acta, 47: 109–124.

Poli, G. and Tommasini, S., 1989. Complex evolution and crystallization history in basic and acid intrusions: the case study of Punta Falcone (Northern Sardinia, Italy). In: Continental Magmatism, abstract. IAVCEI General Assembly, New Mexico Bureau of Mines and Minerals Resources, Bull. 131, 216 pp.

Poli, G., Manetti, P., Peccerillo, A. and Cecchi, A., 1977. Determinazione di alcuni elementi del gruppo delle terre rare in rocce silicatiche per attivazione neutronica. Rend. Soc. Ital. Mineral. Petrol., 33: 755–763.

Poli, G., Ghezzo, C. and Conticelli, S., 1989. Geochemistry of granitic rocks from the Hercynian Sardinia–Corsica Batholith: implication for magma genesis. Lithos, 23: 247–266.

Robinson, P., Schumacher, J.C. and Spear, F.S., 1982. Formulation of electron probe analyses. In: D.R. Veblen and P.H. Ribbe (Editors), Reviews in Mineralogy: Amphiboles, Petrology and Experimental Phase Relations. Mineral. Soc. Am., 9B: 6–9.

Rose, W.I., Grant, N.K. and Easter, J., 1979. Geochemistry of the Los Chocoyos ash, Quezalteuango Valley, Guatemala. Geol. Soc. Am. Spec. Pap., 180: 87–99.

Shaw, H.R., Smith, R.L. and Hildreth, W., 1976. Thermogravitational mechanisms for chemical variations in zoned magma chambers. Geol. Soc. Am., Abstr. Progr., 8: 1102.

Stormer, J.C. and Nicholls, J., 1978. XLFRAC: a program for the interactive testing of magmatic differentiation models. Comput. Geosci., 4: 143–159.

Streckeisen, A. and Le Maitre, R.W., 1979. A chemical approximation to the modal QAPF classification of the igneous rocks. Neues Jahrb. Mineral. Abh., 136: 169–206.

Sultan, M., Batiza, R. and Sturchio, N.C., 1986. The origin of small scale geochemical and mineralogic variations in a granite intrusion. Contrib. Mineral. Petrol., 93: 513–523.

Taylor, R.P., Strong, D.F. and Fryer, B.J., 1981. Volatile control of contrasting trace element distributions in peralkaline granitic and volcanic rocks. Contrib. Mineral. Petrol., 77: 267–271.

Tindle, A.G. and Pearce, J.A., 1981. Petrogenetic modelling of in situ fractional crystallization in the Zoned Loch Doon Pluton, Scotland. Contrib. Mineral. Petrol., 78: 196–207.

Tommasini, S., 1987. Il Batolite Sardo–Corso: studio della massa basica di Punta Falcone. Unpubl. Thesis, University of Florence, Florence, 120 pp.

Verneries, J., Joron, J.L., Treuil, M., Coulon, C. and Dupuy, C., 1977. Coefficient de partage de quelques éléments en trace entre plagioclase et verre dans les ignimbrites, implications pétrogénétiques. Chem. Geol., 19: 309–325.

Wall, V.J., Clemens, J.D. and Clarke, D.B., 1987. Models for granitoid evolution and source composition. J. Geol., 95: 731–749.

White, A.J.R. and Chappell, B.W., 1977. Ultrametamorphism and granitoid genesis. Tectonophysics, 43: 7–22.

Wones, D.R. and Eugster, H.P., 1965. Stability of biotite: experiment, theory and application. Am. Mineral., 50: 1228–1272.